Application of the ONIOM-Molecular Dynamics Method to the Organometallic Reaction Cis-$(H)_2Pt(PR_3)_2 \rightarrow H_2 + Pt(PR_3)_2$ (R = H, Me, Ph, and t-Bu). An Insight into the Dynamical Environmental Effects

Toshiaki Matsubara*

Center for Quantum Life Sciences and Graduate School of Science, Hiroshima University, 1-3-1, Kagamiyama, Higashi-Hiroshima 739-8530, Japan

Received: April 9, 2008; Revised Manuscript Received: July 1, 2008

The ONIOM-molecular dynamics (MD) method, which we recently developed, is applied to one of representative organometallic reactions, *cis*-$(H)_2Pt(PR_3)_2 \rightarrow H_2 + Pt(PR_3)_2$ (R = H, Me, Ph, and t-Bu) to give an insight into the dynamical effects of the environment on the reaction. We adopted the two-layered ONIOM methodology and divided the system into the inner part of *cis*-$(H)_2Pt(PH_3)_2$ and the outer part of the others. The inner and outer parts are treated by the quantum mechanics (QM) method at the HF level of theory and the molecular mechanics (MM) method with the MM3 force field, respectively. The ONIOM-MD simulations show that the thermal motion of the outer part increases the magnitude of the energy fluctuations of the inner part and promotes the H_2 elimination reaction. These dynamical environmental effects increase in the order, t-Bu > Ph > Me > H, indicating that the reactivity of *cis*-$(H)_2Pt(PR_3)_2$ increases in the same order. These results are also supported by an equation derived from the Arrhenius' equation (Matsubara's equation). The snapshots of the reaction for R = t-Bu clearly indicate the new feature of the H_2 elimination process.

1. Introduction

We recently developed the ONIOM-MD method,[1] where the direct MD simulations are performed calculating the energy and its gradient by the ONIOM method[2−8] on the fly. The ONIOM-MD method is a very powerful tool to analyze the environmental effects including the thermal motion. We have applied this method to the realistic model of the enzyme and clarified that the thermal motion of the amino acid residue environment strongly perturbs the geometry and energy of the substrate trapped in the pocket of the active site and affects the elementary step of the catalytic reaction.[1,9,10] We have also successfully simulated the rate-determining step of the enzymatic reaction of cytidine deaminase by the ONIOM-MD method taking account of the thermal motion of the envronment.[9]

About a decade ago, we applied the ONIOM method to the various organometallic reactions,[4,11−13] and revealed the environmental effects on the reaction. In these cases, the steric effect of the substituents on the active site determines the reactivity and selectivity of the reaction. We first applied the ONIOM method to one of the representative elementary reactions, $H_2 + Pt(PR_3)_2 \rightarrow$ *cis*-$(H)_2Pt(PR_3)_2$ (R = H, Me, Ph, and t-Bu). Here, the active part of the system, $H_2 + Pt(PH_3)_2 \rightarrow$ *cis*-$(H)_2Pt(PH_3)_2$, was handled by the ab initio MO method, and the remainder was treated by the MM3 molecular mechanics force field. The geometries of the equilibrium and transition states structures were fully optimized, and the potential energy surface was determined. The ONIOM calculations showed that the reactivity of $Pt(PR_3)_2$ strongly depends on the substituent R of the phosphine ligand. The oxidative addition of H_2 is exothermic with a low energy barrier in the less congested system for R = H, Me, and Ph, while it is endothermic with a high energy barrier in the sterically congested system for R = t-Bu. This calculated result by the ONIOM method is consistent with the following experimental results.

Otsuka and co-workers have reported that the Pt(0) complex $Pt[(t\text{-}Bu)_2P(CH_2)_3P(t\text{-}Bu)_2]$ with the chelating phosphine ligand reacts with H_2 in toluene to produce the *cis*-dihydrido product *cis*-$(H)_2Pt[(t\text{-}Bu)_2P(CH_2)_3P(t\text{-}Bu)_2]$.[14] The two-coordinate phosphine complexes PtL_2 (L = $P(c\text{-}C_6H_{11})_3$, $P(i\text{-}Pr)_3$) also react with H_2 at room temperature under atmospheric pressure to finally give the stable *trans*-PtH_2L_2 product.[15] However, in the case of L = $P(t\text{-}Bu)_3$ and $PPh(t\text{-}Bu)_2$, H_2 practically does not add under the same reaction conditions. The reactivity of PtL_2 toward H_2 qualitatively increases in the order, $P(t\text{-}Bu)_3 \ll PPh(t\text{-}Bu)_2 < P(c\text{-}C_6H_{11})_3 < P(i\text{-}Pr)_3$.

The previous ONIOM calculations have demonstrated that the steric effect of the environment significantly changes the potential energy surface. This might be one of reasons to determine the reactivity. However, the thermal motion of the environment should be taken into account to describe more realistic feature of the reaction, as our previous ONIOM-MD simulations have evidenced that the thermal motion is a crucial factor of the environmental effects for enzymes. For example, dynamical environmental effects on the active site would be readily expected for the H_2 elimination, *cis*-$(H)_2Pt(PR_3)_2 \rightarrow H_2 + Pt(PR_3)_2$. In this case, the inner (active) part of *cis*-$(H)_2Pt(PH_3)_2$ would be affected by the thermal motion of the outer part of the substituent R, because the inner part is surrounded by the outer part, as presented in Scheme 1. This situation of the inner part is similar to that of the substrate trapped in the pocket of the enzyme.

As mentioned above, according to the ONIOM method, the sterically congested t-Bu substituent makes the cis-product unstable, and then the oxidative addition of H_2 become difficult. On the other hand, the less congested H, Me, and Ph substituents readily lead to the cis-product. Therefore, the H_2 reductive elimination, *cis*-$(H)_2Pt(PR_3)_2 \rightarrow H_2 + Pt(PR_3)_2$ (R = H, Me,

* To whom correspondence should be addressed. E-mail: matsu05@hiroshima-u.ac.jp.

10.1021/jp803070t CCC: $40.75
Published on Web 09/04/2008

SCHEME 1

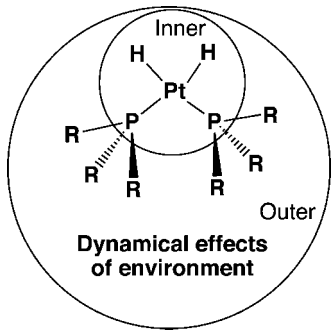

Ph, and t-Bu), would be the most facile in the case of the congested substituent t-Bu. However, the dynamical aspects of the environmental effects still remain unrevealed, and the realistic feature of the reaction process including the thermal motion has not been clarified. In this study, we applied the ONIOM-MD method to one of typical organometallic reactions, *cis*-$(H)_2Pt(PR_3)_2 \rightarrow H_2 + Pt(PR_3)_2$ (R = H, Me, Ph, and t-Bu), and gave a further insight into the environmental effects, taking account of the thermal motion. As a result, we successfully found the dynamical factor of the environmental effects that control the reactivity and revealed a new feature of the H_2 elimination process.

2. Computational Details

We adopted the two-layered ONIOM methodology for the system, *cis*-$(H)_2Pt(PR_3)_2 \rightarrow H_2 + Pt(PR_3)_2$ (R = Me, Ph, and t-Bu). The inner part is *cis*-$(H)_2Pt(PH_3)_2 \rightarrow H_2 + Pt(PH_3)_2$, where all the P−C bonds were cut and the formed dangling bonds were capped with the H atoms. The substituents of R = Me, Ph, and t-Bu, which would affect the inner (active) part, are involved in the outer part. When R is H, the system corresponds to the inner part. This ONIOM partition is the same as that previously used for this system.[4] The inner part was treated by the quantum mechanical (QM) method at the Hartree−Fock (HF) level of theory. We used the basis set, which consists of the relativistic effective core potential (ECP) replacing the core electrons up to 4f with the valence double ζ (8s,6p,3d)/[3s,3p,2d] basis functions by Hay−Wadt for Pt,[16] 6−311G** for H of dihydrogen molecule and hydride, and the standard STO-2G for PH_3. This basis set, which is referred to as BSI below, is almost the same as that used previously.[4] In the previous study, we also used the MP2 level of theory as the QM method with a higher basis set to improve the energy. However, the use of the MP2 level in the MD simulation makes the calculations difficult due to the high computational cost. Since the tendency in the potential energy surface of R = H, Me, Ph, and t-Bu is similar even at the HF level, in this study, we adopted not the MP2 level but the HF level to avoid the problem of the computational cost. The outer part was treated by the molecular mechanics (MM) method using the MM3 force field parameters. The van der Waals parameters reported by Rappe et al. are used for the Pt atom.[17] The torsional contributions associated with dihedral angles involving Pt are set to zero. For the other atoms, the standard MM3 parameters were used. The ONIOM energy is expressed by the sum of the QM and MM energies for the inner and outer parts, and the energy of the outer part is defined as follows.

$$E(\text{ONIOM}) = E(\text{QM,inner}) + E(\text{MM,outer}) \quad (1)$$

$$E(\text{MM,outer}) = E(\text{MM,entire}) - E(\text{MM,inner}) \quad (2)$$

The ONIOM-molecular dynamics (MD) method implemented in the HONDO-2001 program[18] was used for the molecular dynamics (MD) simulations for R = Me, Ph, and t-Bu. In the ONIOM-MD method, the direct MD simulation is performed calculating the ONIOM energy and its gradient on the fly. The time evolution of the nuclei was performed with the Beeman algorithm.[19] The simulations were run under the constant temperature with a time step of 1 fs. A Berendsen thermostat[20] with a coupling constant of 100 fs was used to keep the temperature constant. For R = H, the direct QM-MD simulations were performed similarly, calculating the energy and its gradient by the QM method on the fly. The temperature was increased up to 900 K to observe the H_2 elimination during 100 ps, although the experiment was performed at room temperature. The geometry optimizations were performed by the QM method for R = H, and by the ONIOM-MD method for R = Me, Ph, and t-Bu by solving the Newton's equations of motion at zero Kelvin. The nuclei with the initial velocities of zero start to move on the potential energy surface downward. The velocities generated during moving along the potential energy surface are always maintained extremely small by the velocity scaling of the Berendsen thermostat set to be zero. The nuclei slowly come close to the minimum of the potential energy surface and finally stop at the minimum with the velocities of zero. The transition states of the reactions, *cis*-$(H)_2Pt(PR_3)_2 \rightarrow H_2 + Pt(PR_3)_2$ (R = H, Me, Ph, and t-Bu), were determined by the plot of the energy of the system versus the H−H distance of the dihydrido ligands. The data collected every 10 fs from 5 to 80 ps were used to calculate the average, standard deviation of the geometric parameters, energy, and force, unless otherwise noted, because the potential energy of the entire system as well as the temperature becomes almost constant after 5 ps. The variance σ^2 and the standard deviation σ are defined as follows.

$$\sigma^2 = \frac{1}{n}\sum_{i=1}^{n}(X_i - \overline{X})^2 \quad (3)$$

$$\sigma = \sqrt{\frac{1}{n}\sum_{i=1}^{n}(X_i - \overline{X})^2} \quad (4)$$

3. Results and Discussion

3.1. Optimized Structures and Potential Energy Surfaces. We at first optimized the reactants, transition states, and products and determined the potential energy surface of the H_2 elimination reaction, *cis*-$(H)_2Pt(PR_3)_2 \rightarrow H_2 + Pt(PR_3)_2$ (R = H, Me, Ph, and t-Bu) by the QM and ONIOM-MD methods. The conformations of the reactants *cis*-$(H)_2Pt(PR_3)_2$ (R = Me, Ph, and t-Bu) (Figure S1) are quite similar to those obtained by the ONIOM method previously, which have C_{2v} symmetry for R = Me and C_2 symmetry for R = Ph, t-Bu. Because of these symmetries, only one of two geometric parameters is presented for the Pt−P and Pt−H distances below except some cases. The geometrical parameters of the reactants, transition states, and products and the potential energy surfaces calculated by the ONIOM-MD method well reproduce those calculated previously by the ONIOM method (Tables S1 and S2).

The steric effect of the bulky substituent R = t-Bu is reflected in some geometric parameters. When we look at *cis*-$(H)_2Pt[P(t\text{-}Bu)_3]_2$, this effect is the most obvious. The Pt−P distance for R = t-Bu is stretched by 0.063−0.080 Å compared to those for the other substitutes R = H, Me, and Ph. The ∠P−Pt−P angle is also increased to 124.6° for R = t-Bu. These obvious change in the geometry for R = t-Bu would be attributed to the strong steric repulsion between two $P(t\text{-}Bu)_3$ ligands. The H−Pt−H plane also deviates from the P−Pt−P plane as shown by the ∠H−H−Pt−P dihedral angle larger than 0°, because two

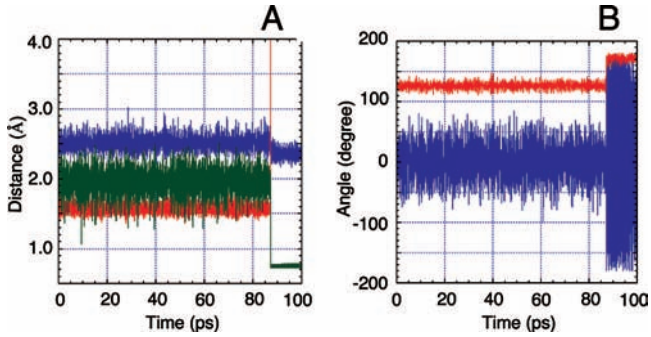

Figure 1. Changes in the geometric parameters (Å and deg) in the reaction *cis*-$(H)_2Pt[P(t\text{-}Bu_3)_2] \rightarrow H_2 + Pt[P(t\text{-}Bu_3)_2]$ during the ONIOM-MD simulation at 900 K. In A, blue: d(Pt1−P2), red: d(Pt1−H4), and green: d(H4−H5). In B, blue: ∠H5−H4−Pt1−P3 and red: ∠P2−Pt1−P3.

hydrido ligands avoid the P−Pt−P plane where enough space cannot be obtained.

The H_2 elimination from *cis*-$(H)_2Pt(PR_3)_2$ is exothermic only for R = t-Bu and is endothermic for the other R = H, Me, and Ph. This dramatic change in the energetics is readily understood from the energy change in the environment. The energy of the outer part E(MM,outer) keep decreasing during the reaction in the case of R = t-Bu, because the steric repulsion between two $P(t\text{-}Bu)_3$ is much reduced with the increase in the ∠P−Pt−P angle as presented below.

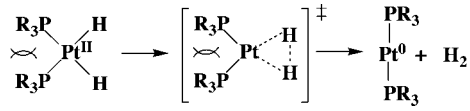

This decrease in the energy of the outer part makes the reaction exothermic and reduces the energy barrier. The similar environmental effects does not exist for R = Ph, because the Ph planes can avoid the mutual steric contact by their rotation even in the reactant.

3.2. ONIOM-Molecular Dynamics (MD) Simulations of *cis*-$(H)_2Pt(PR_3)_2 \rightarrow H_2 + Pt(PR_3)_2$ (R = H, Me, Ph, and t-Bu). The ONIOM-MD simulations of *cis*-$(H)_2Pt(PR_3)_2 \rightarrow H_2 + Pt(PR_3)_2$ (R = H, Me, Ph, and t-Bu) were performed at 300 K, 600 K, and 900 K, starting from the optimized structures of *cis*-$H_2Pt(PR_3)_2$ mentioned in the previous section. As far as we tried, the H_2 elimination occurred only when R is t-Bu in the simulations during 100 ps. The changes in the geometric parameters for R = t-Bu in an ONIOM-MD simulation at 900 K are shown in Figure 1. Figure 1 shows that the H_2 eliminates at 87.2 ps. With the release of the H_2 molecule, the related geometric parameters suddenly change. The H4−H5 distance decreases, while the Pt1−H4 distance increases (Figure 1A). The fluctuations of the H4−H5 distance also suddenly decrease after the H_2 elimination. The average of the Pt1−P2 distance of 2.522 Å decreases to 2.357 Å, and its standard deviation also decreases from 0.099 Å to 0.064 Å, because the large steric repulsion between two $P(t\text{-}Bu)_3$ ligands reduces with the increase in the ∠P2−Pt1−P3 angle. As shown in Figure 1B, the angle ∠P2−Pt1−P3 increases to 180° after the H_2 elimination.

We focused on the change in the geometric parameters in the short time domain from 86.5 to 87.5 ps where H_2 eliminates. Figure 2C shows that the H_2 bond is at first formed at 87.16 ps. At this moment, the H4−H5 already shortens to 0.781 Å. On the other hand, the distances of the Pt1−H4 and Pt1−H5 are 1.883 Å and 1.811 Å, respectively, which are not significantly stretched. The angle ∠P2−Pt1−P3 of 138.2° is still within its fluctuations (see Figure 2A). Here, it is very interesting that the dihedral angle ∠H5−H4−Pt1−H3 is 82.0° as mentioned below. This fact indicates that the H_2 axis is nearly perpendicular to the P2−Pt1−P3 plane. However, the fluctuations of the dihedral angle ∠H5−H4−Pt1−H3 become small and close to zero just before 87.16 ps. It should be noted that one of terminal H (H62 in Figure 3) of t-Bu comes close to the Pt just before the H_2 elimination as shown in Figure 2. Other simulations also similarly showed the approach of the terminal H of t-Bu to the Pt (see Figures S2 and S3). This approach of the terminal H of t-Bu occurs even at the room temperature (Figure S4).

The snapshots of the H_2 elimination process are presented in Figure 3. At 87.14 ps, two hydrido ligands are almost on the P2−Pt1−P3 plane and the H4−H5 distance is 1.658 Å. Although the H4−H5 distance is shortened to 1.072 Å at 87.15 ps, two hydrido ligands are still almost on the P2−Pt1−P3 plane. However, at the next moment at 87.16 ps, the H_2 axis suddenly rotates to become perpendicular to the P2−Pt1−P3 plane and the H_2 molecule is formed on the Pt as shown by the H4−H5 distance of 0.781 Å. This H_2 formation on the Pt is reasonably understood, because the electron back-donation from the Pt dπ orbital to the H_2 σ* orbital shown below is broken by the rotation of the H_2.

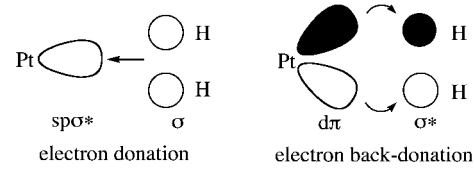

The formed H_2 still interacts with the Pt with the Pt1−H4 distance of 1.883 Å and the Pt1−H5 distance of 1.811 Å because of electron donation from the H_2 σ orbital to the Pt spσ* orbital. Next, this electron donative interaction is broken by the attack of the H(t-Bu) atom. At 87.17 ps, the Pt−H(t-Bu) distance is shortened to 1.887 Å, and then one of the Pt−H distances is elongated up to 2.394 Å. As one can notice, the H(t-Bu) stays close to the Pt during the H_2 elimination, keeping the Pt−H(t-Bu) distance less than 2.3 Å. At 87.18 ps, the H_2 is detached and it goes away from the Pt after 87.19 ps. It should be noted that the H_2 rotates around the axis that penetrates the midpoint of the H_2 and the Pt throughout the H_2 elimination reaction. A similar H_2 elimination process was observed in another simulation (Figure S5). However, the H_2 molecule does not always rotate in the H_2 elimination. When an enough energy provided to the H_2 molecule, two Pt−H distances are elongated at the same time and the H_2 molecule is detached from the Pt atom without the significant rotation of the H_2 as presented in Figure S6. But the H(t-Bu) atom contributes to the H_2 elimination in any case. This process of the H_2 elimination with the contribution of the H(t-Bu) atom is a new fact revealed by the ONIOM-MD method.

The QM and MM energies of the inner and outer parts and the ONIOM energy of the entire system are also presented together in Figure 3. At a glance, we cannot find any significant fact in the MM and ONIOM energies. These values seem to change randomly by their fluctuations. However, the change in the QM energy of the inner part showed an energy barrier in this time domain, the value at the top being less than the maximum in the energy change of the inner part as presented in Figure 4. The energy reaches the top of the mountain at 87.16 ps, where the axis of H_2 formed on the Pt atom becomes

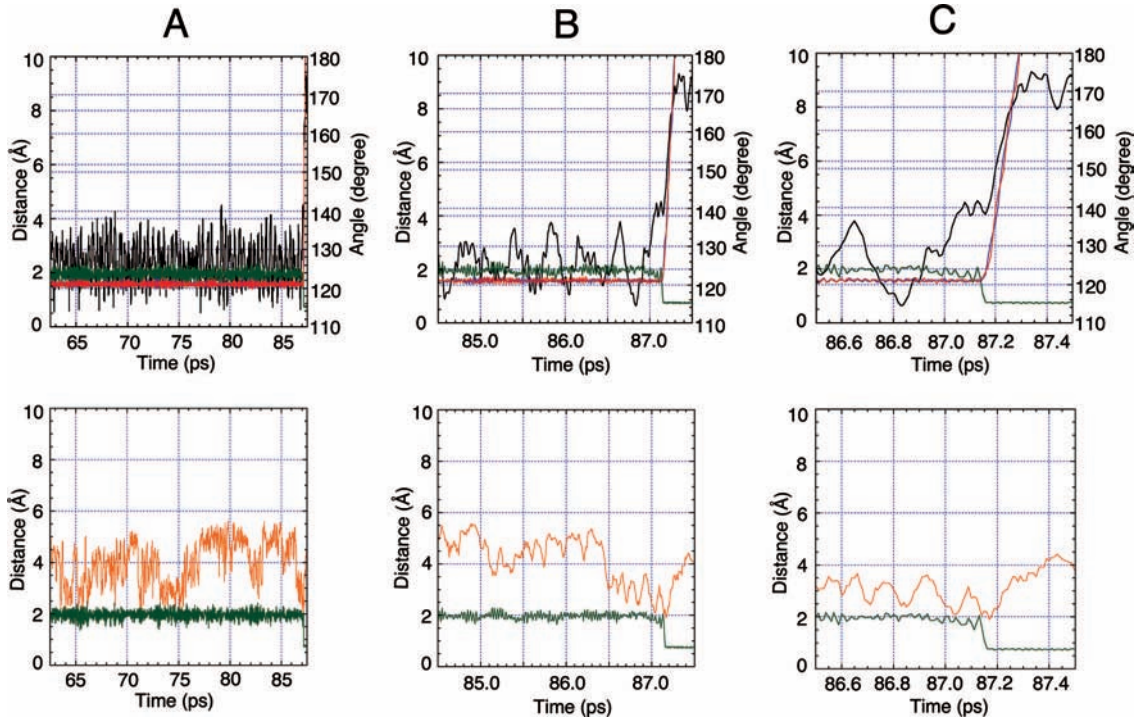

Figure 2. Changes in the geometric parameters in the reaction *cis*-$(H)_2Pt[P(t\text{-}Bu_3)_2] \rightarrow H_2 + Pt[P(t\text{-}Bu_3)_2]$ during the ONIOM-MD simulation at 900 K. The color of the lines represents the geometric parameters as follows: red: d(Pt1−H4), blue: d(Pt1−H5), green: d(H4−H5), orange: d(Pt1−H62), and black: ∠P2−Pt1−P3. A, B, and C have a different time scale.

TABLE 1: Average and Standard Deviation of the Selected Geometric Parameters (Å and deg) of *cis*-$(H)_2Pt(PR_3)_2$ (R = H, Me, Ph, and t-Bu) in the QM-MD and ONIOM-MD Simulations at Various Temperatures[a]

	d(Pt1−P2)		d(Pt1−H4)		d(H4−H5)		∠P2−Pt1−P3		∠H5−H4−Pt1−P3	
R	average	standard deviation	average	standard deviation	average	standard deviation	average	standard deviation	average	standard deviation
					300 K					
H	2.400	0.039	1.587	0.019	2.145	0.067	103.5	3.7	0.0	18.2
Me	2.408	0.042	1.592	0.036	2.141	0.091	105.5	3.6	−0.1	27.2
Ph	2.418	0.041	1.596	0.050	2.134	0.096	106.3	3.2	−0.2	26.2
t-Bu	2.485	0.052	1.573	0.036	1.979	0.099	125.4	3.0	1.7	15.5
					600 K					
H	2.411	0.072	1.587	0.025	2.143	0.076	103.2	3.6	0.0	26.0
Me	2.418	0.062	1.597	0.055	2.136	0.146	105.7	4.9	−0.2	41.2
Ph	2.434	0.072	1.596	0.057	2.115	0.134	108.9	5.0	−0.6	34.0
t-Bu	2.501	0.075	1.579	0.057	1.967	0.140	125.9	4.1	0.4	20.8
					900 K					
H	2.410	0.059	1.588	0.026	2.137	0.104	103.0	5.3	−0.2	37.4
Me	2.432	0.085	1.599	0.061	2.125	0.174	106.0	6.1	−0.2	48.6
Ph	2.449	0.088	1.601	0.072	2.103	0.173	110.0	6.1	−0.3	39.8
t-Bu	2.522	0.099	1.582	0.070	1.948	0.177	126.3	5.0	1.2	26.5

[a] The simulations were performed by the QM-MD method for R = H and by the ONIOM-MD method for R = Me, Ph, and t-Bu.

perpendicular to the P2−Pt1−P3 plane. We should keep in mind the fact that the energy difference of 11.3 kcal/mol between the structures at 87.14 and 87.16 ps is smaller than the energy barrier of 24.4 kcal/mol presented in Table S2.

The average and the standard deviation of the geometric parameters of the inner part for R = H, Me, Ph, and t-Bu at the various temperature are presented in Table 1. The tendencies in the geometric parameters among the substituents R = H, Me, Ph, and t-Bu found in the optimized structures similarly appear in the average of the geometric parameters in the ONIOM-MD simulations at any temperature. The magnitude of the standard deviation for the Pt1−P2 distance increases in the order, t-Bu > Ph > Me > H, except in some cases. On the other hand, no tendency seems to exist in the magnitude of the standard deviation of the Pt1−H4 distance and the ∠P2−Pt1−P3 angle. For the standard deviation of the H4−H5 distance, its magnitude is relatively large for R = t-Bu in spite of the short H4−H5 distance, which indicates that the stretch motion of the H4−H5 is strongly perturbed by the motion of the outer part of the bulky t-Bu. Although the average of the dihedral angle ∠H5−H4−Pt1−P3 is almost zero for all the substituents R = H, Me, Ph, and t-Bu, the standard deviation is the smallest for R = t-Bu because of steric restriction of the space on the Pt.

As shown in Figure 2A, the magnitude of the fluctuations of the H4−H5 distance and that of the Pt1−H4 and Pt1−H5 distances repeat the increase and the decrease with a same cycle. It is obvious that the magnitude of the fluctuations of the H4−H5 distance increases when the H(t-Bu) atom comes close to the Pt. It would be rational to think that two hydrido ligands are energetically enhanced through the steric contact of the H(t-

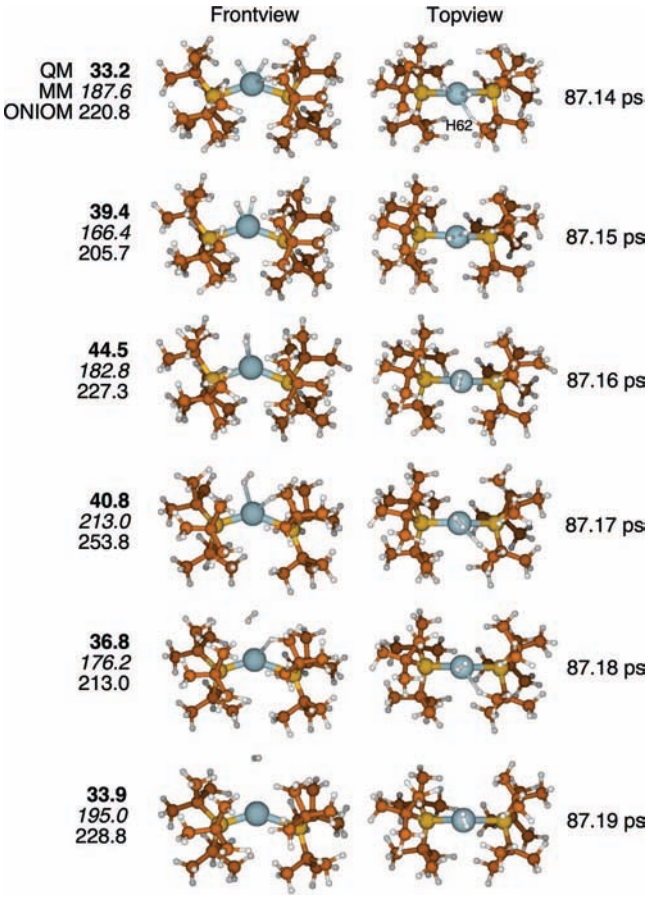

Figure 3. Snapshots of the reaction *cis*-$(H)_2Pt[P(t\text{-}Bu_3)_2]$ → H_2 + $Pt[P(t\text{-}Bu_3)_2]$ in the ONIOM-MD simulation at 900 K. The values (kcal/mol) in the bold, italic, and normal type on the left-hand side are the QM energy of the inner part, the MM energy of the outer part, and the ONIOM energy of the entire system, respectively.

Bu) with the Pt. This approach of the H(t-Bu) atom will also cause a C−H σ donation and prevent the H_2-σ donation to the Pt, if the electronic effect is taken into account. The magnitude of the fluctuations of the ∠P2−Pt1−P3 angle also changes with a cycle. When the H4−H5 distance shortens, the ∠P2−Pt1−P3 angle has to enlarge in order to eliminate H_2. However, before the H_2 elimination takes place at 87.2 ps, both cycles of the changes in the magnitudes of the H4−H5 distance and the ∠P2−Pt1−P3 angle do not match as shown in Figure 2B. Both cycles match each other in the time domain from 87.0 to 87.2 ps just before the H_2 elimination takes place. The H(t-Bu) atom also attacks the Pt for a while after 86.5 ps, until the H_2 eliminates. In the time domain from 87.0 to 87.2 ps where all the factors to eliminate the H_2 are prepared, two hydrido ligands, H4 and H5, start the reaction as shown by the change in the H4−H5 distance. After the H_2 is detached from the Pt at 87.2 ps, the ∠P2−Pt1−P3 angle increases along the downhill energy surface of the outer part (Figure 2C).

The changes in the QM and MM energies of the inner and outer parts and in the ONIOM energy of the entire system in the ONIOM-MD simulation at 900K for R = t-Bu are presented in Figure 4. It is obvious that the QM energy of the inner part of 44.5 kcal/mol at the top of the mountain in the H_2 release at 87.16 ps is not especially high. The ONIOM energy of the entire system as well as the MM energy of the outer part becomes lower after the H_2 elimination, since the strong steric repulsion between two bulky phosphine ligands is reduced. The difference between the average energies before and after the H_2 elimination

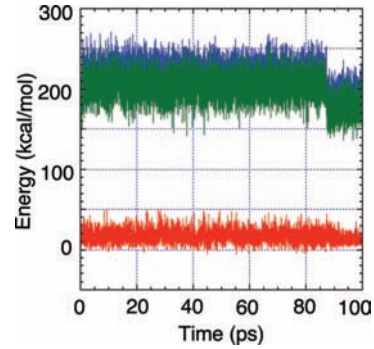

Figure 4. Changes in the potential energies in the reaction *cis*-$(H)_2Pt[P(t\text{-}Bu_3)_2]$ → H_2 + $Pt[P(t\text{-}Bu_3)_2]$ during the ONIOM-MD simulation at 900 K. Blue: ONIOM energy of the entire system, green: MM energy of the outer part, red: QM energy of the inner part.

for the outer part and the entire system are presented in Table 2. In both cases, the energy difference is much larger than those presented in Table S2, because the energy of the outer part is extremely enhanced in energy before the H_2 elimination by the thermal motion of the bulky substituents t-Bu in the restricted space with the small P2−Pt1−P3 angle.

The thermal motion of the bulky t-Bu in the congested space also affects the inner part. The inner part is energetically enhanced before the H_2 elimination, so that the average of the QM energy of the inner part become stable by 3.6 kcal/mol after the H_2 elimination. In contrast, Table S2 shows that the inner part becomes less stable by 6.1 kcal/mol after the H_2 elimination. One will notice that the average of the energy of the inner part is slightly smaller for R = t-Bu than for R = Ph. However, this would be reasonable, if we think that the starting structure in the simulation already has a high energy due to the large P2−Pt1−P3 angle in the case of R = t-Bu. When we look at the relative average energy, the value is much larger for R = t-Bu than for R = Ph. Here, it should be noted that the standard deviation of the QM energy of the inner part is the largest for R = t-Bu at any temperature. In the congested system for R = t-Bu, the inner part is strongly perturbed by the thermal motion of the bulky t-Bu having a huge energy. As a result, the energy fluctuations of inner part increase. When the system becomes less congested after the H_2 elimination, the energy fluctuations of the inner part are reduced.

In order to examine the dynamical effect of the outer part on the inner part in detail, we analyzed the force added to the atom in the inner part from the outer part. As presented in Table 3, the force added to the Pt atom is small for any case of R = Me, Ph, and t-Bu, although both average and standard deviation increases in the order t-Bu > Ph > Me. On the other hand, the force added to the P atom is large. The average of the force increases in the order, t-Bu > Ph > Me as expected. However, the standard deviation is the smallest for t-Bu, because two bulky $P(t\text{-}Bu)_3$ cannot move so much in the congested space.

The force added to two H atoms from the outer part would be very important as a driving force of the H_2 elimination reaction, as Figure 3 shows that the H_2 bond is formed first before the increase in the P2−Pt1−P3 angle. The changes in the forces added to two hydrido ligands from the outer part at 900 K in the cases of R = Me, Ph, and t-Bu are presented in Figure 5. Both H atoms feel large forces in the case of R = t-Bu. After the H_2 elimination, the added forces become zero. The magnitude of the force obviously increase in the order, t-Bu > Ph > Me. As presented in Table 4, the average and standard deviation are the largest for R = t-Bu at any temperature. The

TABLE 2: Average and Standard Deviation of the Energies (kcal/mol) of *cis*-$(H)_2Pt(PR_3)_2$ (R = H, Me, Ph, and t-Bu) in the QM-MD and ONIOM-MD Simulations at Various Temperatures[a]

	E(QM, inner)			E(MM, outer)		E(ONIOM)	
R	average	standard deviation	relative average energy[b]	average	standard deviation	average	standard deviation
			300 K				
H	3.3	0.9	0.0				
Me	5.2	1.7	2.3	17.6	3.0	22.8	3.1
Ph	6.2	2.6	6.5	54.1	4.7	60.2	4.5
t-Bu	5.5	3.9	19.2	66.9	6.0	72.4	5.3
			600 K				
H	7.1	1.8	0.0				
Me	10.7	3.2	4.1	35.0	5.2	45.7	5.6
Ph	12.2	4.6	8.9	109.4	9.2	121.6	9.1
t-Bu	10.9	5.8	20.9	136.0	10.4	146.9	9.9
			900 K				
H	11.3	2.6	0.0				
Me	16.3	4.8	5.5	51.3	7.9	67.6	8.3
Ph	18.4	6.5	10.9	164.7	12.7	183.1	13.2
t-Bu	17.2/13.6	8.1/5.2	23.0	203.7/176.8	15.4/14.1	220.9/190.4	14.4/13.6

[a] The simulations were performed by the QM-MD method for R = H and by the ONIOM-MD method for R = Me, Ph, and t-Bu. The values on the left and right-hand side of the slash for R = t-Bu are calculated by the data collected from 5 to 80 ps and from 90 to 100 ps, respectively. The average energy is relative to the energy at 0 K for each R = H, Me, Ph, and t-Bu. [b] The relative average energy is the average energy relative to the average energy for R = H.

TABLE 3: Average and Standard Deviation of the Forces (kcal/mol\zmd\Å) Added to the Pt and P Atoms of the Inner Part from the Outer Part in the ONIOM-MD simulations of *cis*-$(H)_2Pt(PR_3)_2$ (R = Me, Ph, and t-Bu) at Various Temperatures[a]

	Pt1		P2		P3	
R	average	standard deviation	average	standard deviation	average	standard deviation
			300 K			
Me	0.163	0.015	29.691	13.011	33.114	14.346
Ph	0.555	0.357	35.272	12.322	36.420	13.108
t-Bu	0.800	0.572	56.685	10.047	57.162	10.044
			600 K			
Me	0.160	0.021	43.172	19.508	41.547	18.508
Ph	0.824	1.027	48.868	18.571	48.588	18.358
t-Bu	1.133	1.101	63.227	13.568	63.384	14.067
			900 K			
Me	0.165	0.067	47.732	21.240	50.873	22.913
Ph	1.069	1.508	56.742	21.737	55.513	21.580
t-Bu	1.414/1.577	1.604/1.497	68.016/64.280	16.414/17.720	68.412/63.750	16.484/17.405

[a] The values on the left and right-hand side of the slash for R = t-Bu are calculated by the data collected from 5 to 80 ps and from 90 to 100 ps, respectively.

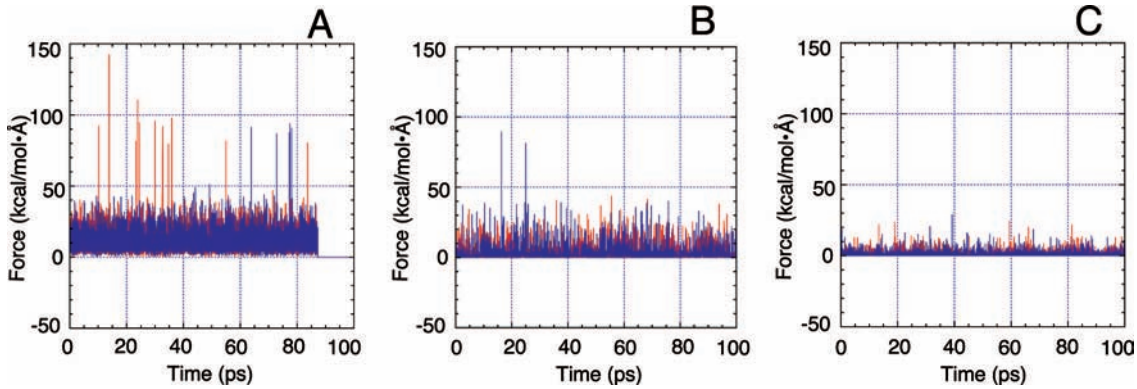

Figure 5. Changes in the forces added to the hydrido ligands of the inner part from the outer part in the reaction *cis*-$(H)_2Pt(PR_3)_2 \rightarrow H_2 + Pt(PR_3)_2$ during the ONIOM-MD simulation at 900 K. A: R = t-Bu, B: R = Ph, and C: R = Me. In A, B, and C, red: H4 and blue: H5.

maximum force is also the largest for R = t-Bu. These tendencies are reflected in the number of the value exceeding 50 kcal/mol·Å at 900 K. The large forces added to two hidrido ligands from the outer part in the case of R = t-Bu would be an important driving force for the H_2 formation. In fact, we can see the effect of the force from the environment on the H−H distance before the H_2 elimination. The frequency that the H−H distance becomes less than 1.5 Å is overwhelmingly large in the case of R = t-Bu (Table S3). The minimum value of the H−H distance is also the smallest for R = t-Bu.

3.3. Evaluation of the Reactivity Using the Magnitude of the Energy Fluctuations. Although the outer part is energetically downhill for R = t-Bu, the inner part itself has to overcome an energy barrier as presented in Table S2. The essential barrier

exits in the inner part. When the inner part overcomes a barrier, the reaction proceeds. *Therefore, we have to assess the reactivity not by the energy barrier of the entire system including the outer part but by the energy barrier of the inner part taking account of the dynamical environmental effects of the outer part caused by the thermal motion.* As mentioned above, the thermal motion of the bulky t-Bu having a huge energy in the congested space makes a driving force of the reaction. After the H_2 is detached from the Pt, the large steric repulsion between two phosphine ligands is reduced by the increase in the ∠P2−Pt1−P3 angle along the downhill energy surface. The dynamical effects of the outer part caused by the thermal motion enlarge the magnitude of the energy fluctuations of the inner part and support to overcome an energy barrier. The energy required to overcome a barrier is provided from the energy fluctuations of the inner part as shown in Figure 4. Therefore, the reaction would become more facile, when the magnitude of the energy fluctuations of the inner part is enlarged by the dynamical effects of the outer part.

Here, we have to consider that the magnitude of the energy fluctuations of the inner part is different among the substituents, R = H, Me, Ph, and t-Bu, of the outer part even at the same temperature. In this sense, not the temperature but the energy fluctuations are essential factors to evaluate the reaction rate. Therefore, we derived an equation, which connects the temperature T to the standard deviation of the energy σ_E, in order to replace the temperature T by the standard deviation of the energy σ_E, in the Arrhenius' equation. The variance of the energy σ_E^2 is written in the following form, since we think a canonical ensemble with the constant temperature.

$$\sigma_E^2 = \langle (E - \langle E \rangle)^2 \rangle = \langle E^2 \rangle - \langle E \rangle^2 \tag{5}$$

The average energy is expressed as follows.

$$\langle E \rangle = \sum_i E_i p_i \tag{6}$$

Here, the probability p_i of E_i in the state i of the system is

$$p_i = \frac{1}{Z} \exp\left(-\frac{E_i}{k_B T}\right) \tag{7}$$

The partition function Z is written as

$$Z = \sum_i \exp\left(-\frac{E_i}{k_B T}\right) \tag{8}$$

Using eq 6, the energy fluctuations are written as

$$\sigma_E^2 = \langle E^2 \rangle - \langle E \rangle^2 = \frac{1}{Z}\left\{\sum_i E_i^2 \exp\left(-\frac{E_i}{k_B T}\right)\right\} - \left\{\frac{1}{Z}\sum_i E_i \exp\left(-\frac{E_i}{k_B T}\right)\right\}^2 \tag{9}$$

On the other hand, the specific heat $C_v = d\langle E \rangle / dT$ is calculated as follows using eq 6.

$$\frac{d\langle E \rangle}{dT} = \frac{d}{dT}\frac{\sum_i E_i \exp\left(-\frac{E_i}{k_B T}\right)}{Z} = \frac{1}{k_B T^2}\left\{\frac{1}{Z}\left(\sum_i E_i^2 \exp\left(-\frac{E_i}{k_B T}\right)\right) - \left(\frac{1}{Z}\sum_i E_i \exp\left(-\frac{E_i}{k_B T}\right)\right)^2\right\} \tag{10}$$

Therefore, the specific heat C_v is written as

$$C_v = \frac{d\langle E \rangle}{dT} = \frac{1}{k_B T^2}\sigma_E^2 \tag{11}$$

According to the principle of equipartition of energy, the average energy is

$$\langle E \rangle = \frac{1}{2} f k_B T \tag{12}$$

Here, f is the number of degree of freedom. The specific heat C_v is, thence, written in another form,

$$C_v = \frac{d\langle E \rangle}{dT} = \frac{1}{2} f k_B \tag{13}$$

Using eqs 11 and 13, we obtain the following equation,

$$\frac{1}{2} f k_B = \frac{1}{k_B T^2}\sigma_E^2 \tag{14}$$

Eq 14 is arranged as follows.

$$T = \sqrt{\frac{2}{f}}\frac{\sigma_E}{k_B} \tag{15}$$

When we use eq 15 in Arrhenius' equation, $k = A \exp(-\Delta E/RT)$, we obtain

$$k = A \exp\left(-\sqrt{\frac{f}{2}}\frac{\Delta E}{\sigma_E}\right) \tag{16}$$

In the derived eq 16 (Matsubara's equation), the rate constant is expressed by the standard deviation of the energy σ_E instead

TABLE 4: Average, Standard Deviation, Maximum Value, and Number of Value Exceeding 50 of the Forces (kcal/mol\zmd\Å) added to the H Atoms of the Inner Part from the Outer Part in the ONIOM-MD Simulations of *cis*-$(H)_2Pt(PR_3)_2$ (R = Me, Ph, and t-Bu) at Various Temperatures

	H4				H5			
R	average	standard deviation	maximum value	number of value exceeding 50	average	standard deviation	maximum value	number of value exceeding 50
				300 K				
Me	0.507	0.515	5.325	0	0.489	0.507	5.746	0
Ph	2.079	1.939	26.930	0	2.017	1.956	23.721	0
t-Bu	10.355	3.970	32.799	0	10.893	3.918	32.853	0
				600 K				
Me	0.713	0.957	13.039	0	0.700	0.973	14.982	0
Ph	2.852	3.299	31.254	0	2.899	3.283	26.838	0
t-Bu	11.113	5.711	97.880	1	10.923	5.544	46.443	0
				900 K				
Me	0.922	1.512	24.676	0	0.956	1.549	29.106	0
Ph	3.406	4.359	43.376	0	3.462	4.854	89.337	3
t-Bu	11.445	7.560	142.481	11	11.372	7.274	93.882	6

of the temperature T. Using eq 16, the ratio of the rate constant for the systems with the different energy fluctuations of the inner part is calculated as follows.

$$\frac{k_a}{k_b} = \frac{\exp\left(-\sqrt{\frac{f^{QM}}{2}}\frac{\Delta E_a^{QM}}{\sigma_{Ea}^{QM}}\right)}{\exp\left(-\sqrt{\frac{f^{QM}}{2}}\frac{\Delta E_b^{QM}}{\sigma_{Eb}^{QM}}\right)} \quad (17)$$

Here, it is assumed that the frequency factors A for two different systems are the same.

We used the standard deviation of the energy of the inner part presented in Table 2 as σ_E^{QM}. The energy barrier of the inner part at the HF (Table S2) and MP2 (Table 4 in ref 4) levels was used as ΔE^{QM}. f is 27. The calculated ratio of the rate constant using eq 17 is presented in Table 5. The qualitative tendencies for the HF and MP2 levels are quite similar. As expected, the reactivity is much larger for R = t-Bu than for the other R = H, Me, and Ph. For example, the rate constant for R = t-Bu is more than 45 times larger than that for R = Ph at the MP2 level at 900 K. The rate constant increases in the order, t-Bu > Ph > Me > H, at any temperature.

The standard deviation of the energy of *cis*-$(H)_2Pt(PR_3)_2$ presented in Table 2 are calculated smaller compared to that calculated by the eq 18. The standard deviation of the energy of *cis*-$(H)_2Pt(PH_3)_2$ is in principle calculated to be 2.2, 4.4, and 6.6 kcal/mol at 300, 600, and 900 K, respectively, according to the eq 18.

$$\sigma_E = k_B T\sqrt{\frac{f}{2}} \quad (18)$$

This fact might make the rate constant smaller than that we expected especially for R = H, because the rate constant is very sensitive to the standard deviation of the energy in eq 16. The average energies for *cis*-$(H)_2Pt(PH_3)_2$ presented in Table 2 are also smaller than those calculated by eq 12 (see Table S4). On the other hand, the average energies of the outer part and entire system for *cis*-$(H)_2Pt(PR_3)_2$ (R = Me, Ph, and t-Bu) are nearly the same as those calculated by eq 12.

TABLE 5: Ratio of the Rate Constant of the Reaction for R = H, Me, Ph to that for R = t-Bu calculated at the Various Temperature[a]

	ratio 1		ratio 2	
R	HF	MP2	HF	MP2
		300 K		
H	1.33×10^{-1}	4.66×10^{-3}	3.93×10^{-36}	1.38×10^{-29}
Me	1.44×10^{-3}	4.66×10^{-3}	2.63×10^{-17}	9.88×10^{-13}
Ph	1.03×10^{-3}	3.33×10^{-3}	3.10×10^{-8}	2.72×10^{-6}
t-Bu	1.00	1.00	1.00	1.00
		600 K		
H	3.65×10^{-1}	6.82×10^{-2}	1.04×10^{-16}	5.88×10^{-14}
Me	3.79×10^{-2}	6.82×10^{-2}	3.99×10^{-8}	4.01×10^{-6}
Ph	3.21×10^{-2}	5.77×10^{-2}	6.71×10^{-4}	3.98×10^{-3}
t-Bu	1.00	1.00	1.00	1.00
		900 K		
H	5.11×10^{-1}	1.67×10^{-1}	1.25×10^{-11}	8.94×10^{-10}
Me	1.12×10^{-1}	1.67×10^{-1}	2.51×10^{-5}	4.30×10^{-4}
Ph	1.01×10^{-1}	1.49×10^{-1}	6.46×10^{-3}	2.19×10^{-2}
t-Bu	1.00	1.00	1.00	1.00

[a] The ratios 1 and 2 were calculated by the eq 19 and 17, respectively.

We also calculated the ratio of the rate constant according to the Arrhenius' equation as follows using the energy barrier of the inner part and the temperature of 300, 600, and 900 K.

$$\frac{k_a}{k_b} = \frac{\exp\left(-\frac{\Delta E_a^{QM}}{RT}\right)}{\exp\left(-\frac{\Delta E_b^{QM}}{RT}\right)} \quad (19)$$

Since the environmental effects of the sterically congested t-Bu substituent reduce the energy barrier of the inner part, the reaction becomes facile in the case of R = t-Bu as presented in Table 5. But when we take account of the dynamical environmental effects through the standard deviation of the energy of the inner part, the reaction for the sterically congested t-Bu substituent becomes much more facile as mentioned above. The inner part is just thought to be embedded in a bath of the outer part and is heated by the thermal motion of the sterically congested substituents of the outer part. We can calculate the temperature of the inner part by eq 15 using the standard deviation of the energy of the inner part. The temperature of the inner part was heated higher by 160−220 K for R = t-Bu than for R = Ph in each temperature as presented in Table S5. This is reflected in the rate constant through the standard deviation of the energy in eq 16. These results explicitly show the dynamical effects of the environment of the sterically congested substutuent of t-Bu.

4. Concluding Remarks

We recently developed the ONIOM-molecular dynamics (MD) method integrating the ONIOM method with the MD method to apply it to the biomolecular system such as enzymes where the thermal motion is thought to be an important factor of their function. We have applied the ONIOM-MD method to cytidine and cytosine deaminase and have clarified the effect of the thermal motion of the environment on the reaction of the substrate inside the pocket of the active site. It is thought that such dynamical environmental effects generally play an important role in the reaction system surrounded by an environment. In this study, we therefore applied the ONIOM-MD method to the representative organometallic reaction, *cis*-$(H)_2Pt(PR_3)_2 \rightarrow H_2 + Pt(PR_3)_2$ (R = H, Me, Ph, and t-Bu), and examined the dynamical environmental effects of the substituents of the ligands on the reaction of the active site taking account of the thermal motion.

The ONIOM-MD simulations showed that the thermal motion of the substituents of the ligands increases the magnitude of the energy fluctuations of the active part. These dynamical effects of the environment enhance the reaction of the active site, because the energy required to overcome the barrier is provided from the energy fluctuations. In order to evaluate the contribution of the energy fluctuations to the reactivity, we derived an equation (Matsubara's equation) from the Arrhenius' equation where the energy fluctuations instead of temperature are connected to the rate constant. Using this equation, we found that the reactivity increases in the order t-Bu > Ph > Me > H.

The snapshots of the reaction for R = t-Bu clearly indicated the new feature of the H_2 elimination. The H_2 formation first takes place on the Pt by the approach of two hydrido ligands to each other and their rotation, with the support of the force from the outer part, which is a driving force of the reaction. The formed H_2 is released from the Pt by the attack of a terminal H of t-Bu to the Pt. After the release of the H_2, the angle ∠P2−Pt1−P3 enlarges. When some factors required for the

reaction successfully collaborate, the reaction starts and the H_2 elimination is completed. Thus, the ONIOM-MD method showed that the dynamical environmental effects are crucial factors on the organometallic reaction and brought us a new finding of the reaction process.

Acknowledgment. This study was supported in part by grants from the Ministry of Education, Culture, Sports, Science and Technology of Japan.

Supporting Information Available: Figures S1−S6 and Tables S1−S5. This material is available free of charge via the Internet at http://pubs.acs.org.

References and Notes

(1) Matsubara, T.; Dupuis, M.; Aida, M. *Chem. Phys. Lett.* **2007**, *437*, 138–142.
(2) Maseras, F.; Morokuma, K. *J. Comput. Chem.* **1995**, *16*, 1170–1179.
(3) Matsubara, T.; Sieber, S.; Morokuma, K. *Int. J. Quantum Chem.* **1996**, *60*, 1101–1109.
(4) Matsubara, T.; Maseras, F.; Koga, N.; Morokuma, K. *J. Phys. Chem.* **1996**, *100*, 2573–2580.
(5) Svensson, M.; Humbel, S.; Froese, R. D. J.; Matsubara, T.; Sieber, S.; Morokuma, K. *J. Phys. Chem.* **1996**, *100*, 19357–19363.
(6) Dapprich, S.; Komáromi, I.; Byun, K. S.; Morokuma, K.; Frisch, M. J. *J. Mol. Struct. (THEOCHEM)* **1999**, *461−462*, 1–21.
(7) Vreven, T.; Morokuma, K. *J. Comput. Chem.* **2000**, *21*, 1419–1432.
(8) Morokuma, K. *Bull. Korean Chem. Soc.* **2003**, *24*, 797–801.
(9) Matsubara, T.; Dupuis, M.; Aida, M. *J. Phys. Chem. (B)* **2007**, *111*, 9965–9974.
(10) Matsubara, T.; Dupuis, M.; Aida, M. *J. Comput. Chem.* **2008**, *29*, 458–465.
(11) Nozaki, K.; Komaki, H.; Kawashima, Y.; Hiyama, T.; Matsubara, T. *J. Am. Chem. Soc.* **2001**, *123*, 534–544.
(12) Sahnoun, R.; Matsubara, T.; Yamabe, T. *Organometallics* **2000**, *19*, 5661–5670.
(13) Nozaki, K.; Sato, N.; Tonomura, Y.; Yasutomi, M.; Takaya, H.; Hiyama, T.; Matsubara, T.; Koga, N. *J. Am. Chem. Soc.* **1997**, *119*, 12779–12795.
(14) Yoshida, T.; Yamagata, T.; Tulip, T. H.; Ibers, J. A.; Otsuka, S. *J. Am. Chem. Soc.* **1978**, *100*, 2063.
(15) Yoshida, T.; Otsuka, S. *J. Am. Chem. Soc.* **1977**, *99*, 2134.
(16) Hay, P. J.; Wadt, W. R. *J. Chem. Phys.* **1985**, *82*, 299.
(17) Rappe, A. K.; Casewit, C. J.; Colwell, K. S.; Goddard, W. A., III.; Skiff, W. M. *J. Am. Chem. Soc.* **1992**, *114*, 10024.
(18) Dupuis, M.; Marquez, A.; Davidson, E. R. HONDO 2001, based on HONDO 95.3, available from the Quantum Chemistry Program Exchange (QCPE), Indiana University.
(19) Beeman, D. *J. Comput. Phys.* **1976**, *20*, 130–139.
(20) Berendsen, H. J. C.; Postma, J. P. M.; van Gunsteren, W. F.; DiNola, A.; Haak, J. R. *J. Chem. Phys.* **1984**, *81*, 3684–3690.

JP803070T